ExBox: A Polycyclic Aromatic Hydrocarbon Scavenger

ARTICLE *in* JOURNAL OF THE AMERICAN CHEMICAL SOCIETY · AUGUST 2012

Impact Factor: 12.11 · DOI: 10.1021/ja307360n · Source: PubMed

JACS
JOURNAL OF THE AMERICAN CHEMICAL SOCIETY
Article
pubs.acs.org/JACS

ExBox: A Polycyclic Aromatic Hydrocarbon Scavenger

Jonathan C. Barnes,[†,‡] Michal Juríček,[†,‡] Nathan L. Strutt,[†] Marco Frasconi,[†] Srinivasan Sampath,[†] Marc A. Giesener,[†] Psaras L. McGrier,[†] Carson J. Bruns,[†] Charlotte L. Stern,[†] Amy A. Sarjeant,[†] and J. Fraser Stoddart*[,†]

[†]Department of Chemistry, Northwestern University, 2145 Sheridan Road, Evanston, Illinois 60208, United States

Supporting Information

ABSTRACT: A template-directed protocol, which capitalizes on donor−acceptor interactions, is employed to synthesize a semi-rigid cyclophane (**ExBox**$^{4+}$) that adopts a box-like geometry and is comprised of π-electron-poor 1,4-phenylene-bridged ("extended") bipyridinium units (**ExBIPY**$^{2+}$). **ExBox**$^{4+}$ functions as a high-affinity scavenger of an array of different polycyclic aromatic hydrocarbons (PAHs), ranging from two to seven fused rings, as a result of its large, accommodating cavity (approximately 3.5 Å in width and 11.2 Å in length when considering the van der Waals radii) and its ability to form strong non-covalent bonding interactions with π-electron-rich PAHs in either organic or aqueous media. In all, 11 PAH guests were observed to form inclusion complexes with **ExBox**$^{4+}$, with coronene being the largest included guest. Single-crystal X-ray diffraction data for the 11 inclusion complexes **ExBox**$^{4+}$⊂PAH as well as UV/vis spectroscopic data for 10 of the complexes provide evidence of the promiscuity of **ExBox**$^{4+}$ for the various PAHs. Nuclear magnetic resonance spectroscopy and isothermal titration calorimetric analyses of 10 of the inclusion complexes are employed to further characterize the host−guest interactions in solution and determine the degree with which **ExBox**$^{4+}$ binds each PAH compound. As a proof-of-concept, a batch of crude oil from Saudi Arabia was subjected to extraction with the water-soluble form of the PAH receptor, **ExBox**·4Cl, resulting in the isolation of different aromatic compounds after **ExBox**·4Cl was regenerated.

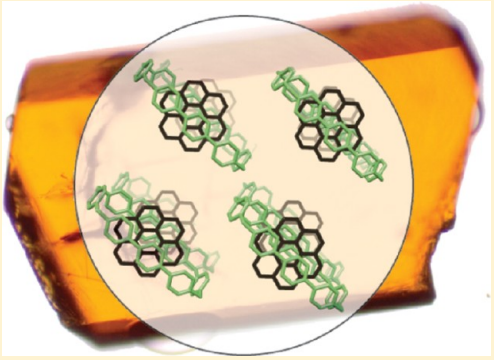

1. INTRODUCTION

A period of 136 years has now passed since the smallest possible polycyclic aromatic hydrocarbon (PAH), naphthalene, was synthesized for the first time.[1] Somewhat less time has passed since the synthesis of the largest well-defined PAH (giant graphene disk containing 222 carbon atoms and 37 fused benzenoid units) was reported a decade ago.[2] During the more than a century-long period in between, PAHs, also known as polyaromatic hydrocarbons,[3] which consist of fused aromatic rings that do not contain heteroatoms or carry substituents, have become an important class of compounds when considering different aspects of life. Not only have they posed questions about the origin of life, as the spectral signatures of anthracene and pyrene have recently been found in the ultraviolet light emitted by the red rectangle nebula,[4] but also somewhere along the way they have become one of the main pollutants and harmful chemical species known on the planet.[5] Yet, without a doubt, they remain among the most beautiful and fascinating classes of organic compounds.[3,6]

The highly characteristic ("fingerprint") optical absorption and emission behavior of PAHs makes it possible to identify unambiguously a compound because the optical as well as the chemical properties of PAHs depend largely on their size and geometry.[6] There are many different combinations of PAHs comprised of the same number of rings, where the number of combinations increases as more rings are added, resulting in different ratios between Clar's aromatic sextets[3] and double bonds not included in the Clar's sextet within a homologous series of molecular compounds. Figure 1 illustrates the Clar's structures of the 11 PAH molecules that were investigated in this work and demonstrates how the overall electronic structure undergoes change within PAH isomers. For example, fully benzenoid triphenylene (containing three aromatic sextets) is extremely stable even under drastic conditions, while its isomer tetracene (containing one aromatic sextet and six non-sextet double bonds) is much more reactive and, compared with triphenylene, possesses a lower band gap.[6]

PAHs can be found naturally in oil, coal, and tar. They are produced as byproducts in combustion processes of fuel, be it fossil fuel or biomass.[7] Being lipophilic, meaning they mix more easily with oil than water, PAHs dispersed into the environment are primarily deposited in soil, sediment, and oily substances, as particulate matter suspended in air, and in water, although to a lesser extent. As a pollutant, they are of concern because some of the smaller (partially water-soluble) PAHs, such as benzo[*a*]pyrene, have been identified as carcinogenic, mutagenic, and teratogenic, and they are widely believed to make a substantial contribution to the overall burden of cancer in humans.[8] The major route of exposure to PAHs for people—

Received: July 26, 2012
Published: August 28, 2012

dx.doi.org/10.1021/ja307360n | *J. Am. Chem. Soc.* 2013, 135, 183−192

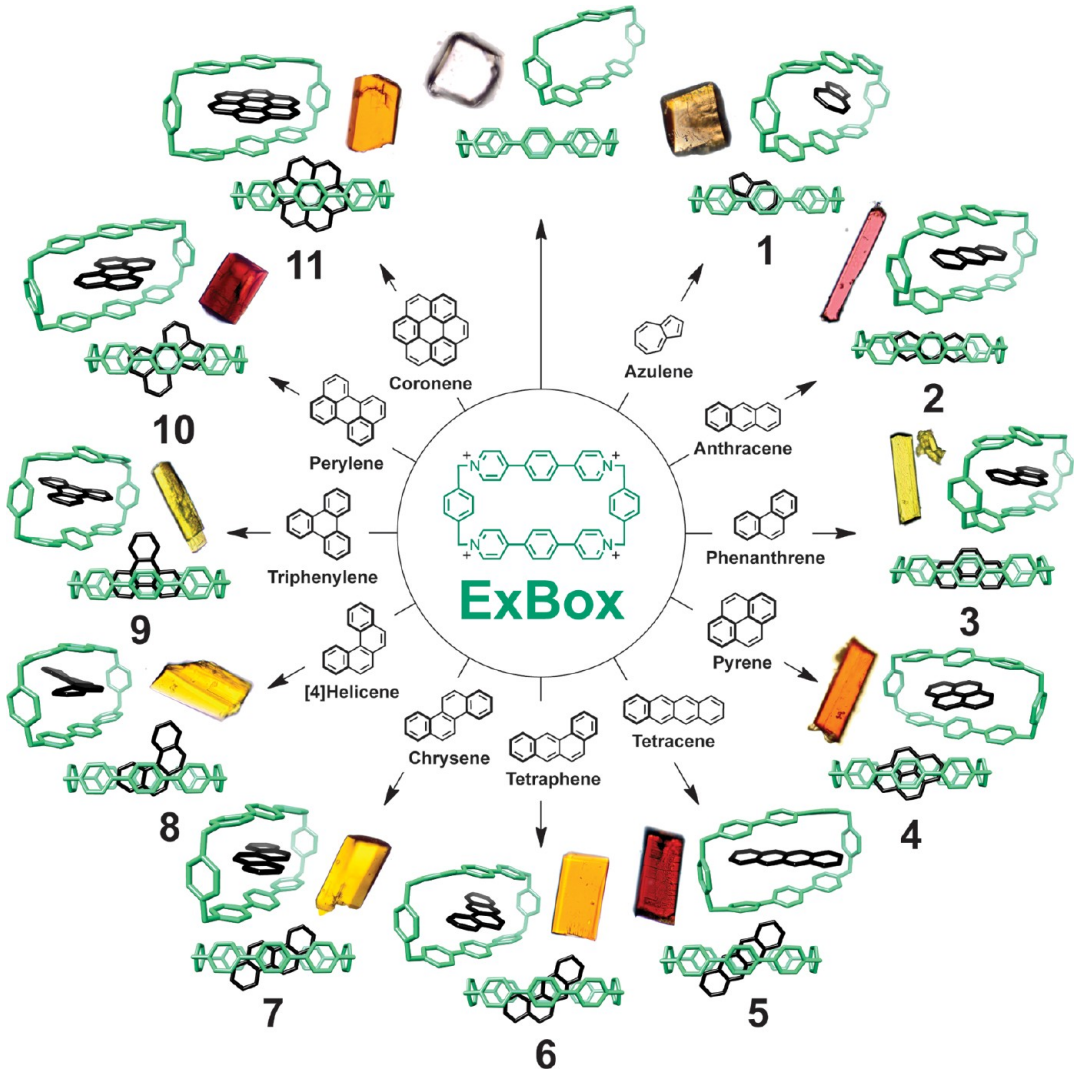

Figure 1. Single-crystal XRD data were obtained for all 11 of the inclusion complexes of **ExBox**⊂guest·4PF_6 (**1**–**11**), along with that of **ExBox**·4PF_6 alone (top). The counterions and solvent molecules are removed for the sake of clarity. In each case, the crystals that were used to obtain the XRD data were photographed under an optical microscope. It is important to note the lack of color in the crystal of **ExBox**·4PF_6 by itself and the presence of different colors for each inclusion complex. The colors arise from charge-transfer interactions between the host and guests, with the exception of **1** because no charge-transfer band was observed in the optical absorption spectrum. The structural formulas depicted with bolded π-bonds highlight the Clar's sextet in each π-electron-rich guest.

nonsmokers—is consumption of food, which can be contaminated from environmental sources as well as industrial or home food processing. The European Food Safety Authority (EFSA), documenting that PAHs are potentially genotoxic and carcinogenic to humans in food, reported[9] that some of the potentially harmful PAHs are present even in fresh fruit.

Considering the potential health risks associated with the release of PAHs into the environment, it is of fundamental importance to understand the supramolecular chemistry[10] surrounding PAHs in order to be able to detect and sequester these harmful molecules. To date, cyclodextrins (CDs)[11] have been used most often to isolate PAHs from crude mixtures, although more recently derivatives of calix[*n*]arenes,[12] cholic acid,[13] and metal–ligand diazapyrenium-based metallocycles[14] have been explored as potential suitors for PAHs of different shapes and sizes. It should be noted, however, that the metallocycles described by Quintela et al.[14] incorporate heavy Pd and Pt ligand–metal coordination in order to form supramolecular architectures, which are expensive and would not be ideal from environmental and economical perspectives. Ideally, the PAH receptor should (1) be robust, so it can be used multiple times to extract PAHs, (2) bind a vast range of PAHs which possess a different number of fused benzenoid rings, and (3) be soluble in both organic and aqueous media, whereby the receptor cyclophane can be regenerated easily by way of solvent extraction.

In this article, we describe the synthesis and properties of a macrocyclic organic salt **ExBox**$^{4+}$, which serves as a high-affinity scavenger of an array of PAHs, up to the size of coronene, in both aqueous and organic media (Figure 1). We demonstrate the ability of **ExBox**$^{4+}$ to bind PAHs of different size and shape by means of donor–acceptor interactions on 11 examples of common PAHs ranging in size from two to seven aromatic rings, two of which (tetraphene and chrysene) are known[9] for their mutagenicity/genotoxicity in somatic cells in experimental animals *in vivo*. We present the full solid-state characterization of the inclusion complexes of **ExBox**$^{4+}$ with all 11 PAHs and envisage its potential in the extraction and detection of harmful

dx.doi.org/10.1021/ja307360n | *J. Am. Chem. Soc.* 2013, 135, 183–192

Scheme 1. Reaction Scheme for the Synthesis of ExBox·4PF_6, Starting with the Reported[17] Extended Bipyridine (ExBIPY)

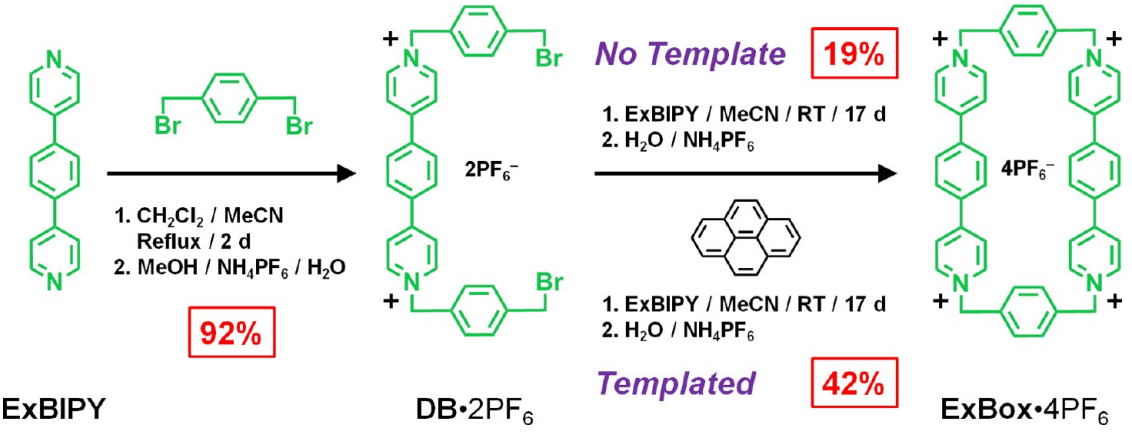

PAHs from the environment. Finally, the potential for the **ExBox**⊃PAH donor−acceptor superstructures to be used in organic field-effect transistors is considered.

2. EXPERIMENTAL SECTION

The full experimental details are provided in the Supporting Information (SI). Below, the most important information is briefly summarized.

Single-Crystal X-ray Diffraction (XRD). Single crystals of **ExBox**·4PF_6 and its complexes **1**−**11** were grown by slow vapor diffusion of *i*Pr_2O into solutions of **ExBox**·4PF_6 (or **ExBox**·4PF_6 and PAH guests (1:1.1)) in MeCN (3.0 mM) over the course of 1 week. Data were collected at 100 K on a Bruker Kappa APEX CCD diffractometer equipped with a Cu Kα microsource with Quazar optics.

Isothermal Titration Calorimetry (ITC). All ITC measurements were performed in dry, degassed MeCN at 298 K. A solution of **ExBox**·4PF_6 in MeCN was used as the host solution in a 1.8 mL cell. Solutions of aromatic guests in MeCN were added by injecting successively 10 μL of titrant over 20 s (25×) with a 300 s interval between each injection. Experiments were repeated three times. Thermodynamic information was calculated using a one-site binding model utilizing data from which the heat of dilution of the guest was subtracted, with the average of three runs reported.

Nuclear Magnetic Resonance (NMR) Spectroscopy. ^{1}H NMR (298 K, 500 MHz) titrations were performed by adding small volumes of a concentrated guest solution/suspension in $CDCl_3$ to a solution of **ExBox**·4PF_6 in CD_3CN. Tetramethylsilane was used as a reference. Significant upfield shifts of the ^{1}H resonances for γ protons were observed and used to determine the association constants (K_a). The K_a values were calculated using Dynafit, a program that employs nonlinear least-squares regression on ligand−receptor binding data. In the case of **10** and **11**, the low solubility of perylene and coronene prohibited the calculation of reliable K_a values. The estimated K_a value for **10** is reported, however, the error is substantial (76%).

Bisbromomethyl(bis-*p*-benzyl-4,4′-(1,4-phenylene)-bispyridine)bis(hexafluorophosphate) (DB·2PF_6). α,α'-Dibromo-*p*-xylene (4.58 g, 17.2 mmol) was added to CH_2Cl_2 (30 mL) in a 250 mL round-bottomed three-neck flask, and the resulting mixture was refluxed while stirring until all of the solid material dissolved. Next, the temperature of the oil bath was raised to 90 °C, allowing the reaction mixture to reflux, while a suspension of **ExBIPY** (400 mg, 1.72 mmol) in MeCN (60 mL) was added in five aliquots slowly over 1 h. After only 30 min, however, a yellow precipitate, indicative of **DB**·2Br formation, began to appear. After heating under reflux for 48 h, the reaction mixture was cooled to room temperature, and the yellow precipitate was collected by filtration and washed with CH_2Cl_2. The yellow solid was dissolved in cold (≤25 °C) MeOH (∼500−750 mL) followed by the addition of NH_4PF_6 (∼100−200 mg) and cold (≤25 °C) H_2O (∼2 L), resulting in the precipitation of pure **DB**·2PF_6 (1.41 g, 92%) that was collected by filtration as a white solid. HRMS-ESI for **DB**·2PF_6: calcd for $C_{32}H_{28}Br_2F_{12}N_2P_2$, m/z = 743.0256 $[M - PF_6]^+$, 597.0536 $[M - 2PF_6]^{2+}$; found, 743.0262 $[M - PF_6]^+$, 597.0538 $[M - 2PF_6]^{2+}$. ^{1}H NMR (500 MHz, CD_3CN, ppm): δ_H 8.66 (AA′ of AA′XX′, J = 6.9 Hz, 4H), 8.19 (XX′ of AA′XX′, J = 6.9 Hz, 4H), 7.97 (s, 4H), 7.40 (AA′ of AA′BB′, J = 8.2 Hz, 4H), 7.31 (BB′ of AA′BB′, J = 8.2 Hz, 4H), 5.58 (s, 4H), 4.46 (s, 4H). ^{13}C NMR (125 MHz, CD_3CN, ppm): δ_C 155.0, 144.3, 139.9, 136.7, 132.9, 129.8, 129.1, 129.1, 125.6, 63.1, 32.3.

Cyclobis(4,4′-(1,4-phenylene)bispyridine-*p*-phenylene)-tetrakis(hexafluorophosphate) (ExBox·4PF_6). Two synthetic routes (Scheme 1), methods A (no template) and B (templated), were employed to prepare the tetracationic cyclophane. *Method A*: **DB**·2PF_6 (312 mg, 0.350 mmol) and **ExBIPY** (81.3 mg, 0.350 mmol) were added to dry MeCN (200 mL) and stirred at room temperature. After 17 days, the reaction was stopped by adding concentrated HCl (2−3 mL), which caused the crude product to precipitate from solution. The precipitate was collected by filtration, dissolved in H_2O, and precipitated again by adding NH_4PF_6 (∼100−200 mg). The solid material was collected by filtration and then subjected to column chromatography using silica gel and 1% NH_4PF_6 in MeCN (w/v) as the eluent. The final product was purified further through recrystallization in MeCN on slow vapor diffusion of *i*PrO_2, yielding pure **ExBox**·4PF_6 (83 mg, 19%) as a white solid. *Method B*: **DB**·2PF_6 (312 mg, 0.350 mmol), **ExBIPY** (81.3 mg, 0.350 mmol), and the template pyrene (212 mg, 1.05 mmol) were added to dry MeCN (200 mL) and stirred at room temperature. After 17 days, the reaction was stopped by adding concentrated HCl (2−3 mL), causing the crude product to precipitate from solution. The yellowish-orange precipitate was collected by filtration and then dissolved in H_2O, followed by extracting 5× with CH_2Cl_2 (200 mL per extraction). This solvent extraction step changes the organic layer from an orange solution to a white suspension, indicating that most, if not all, of the template had been removed. The extracted material was precipitated from solution by adding NH_4PF_6 (∼100−200 mg) before being subjected to column chromatography using silica gel and CH_2Cl_2/MeCN (1:1) and 1% NH_4PF_6 in MeCN (w/v) as the eluents, followed by recrystallization as in the case of nontemplated reaction to yield the pure product (184 mg, 42%) as a white solid. HRMS-ESI for **ExBox**·4PF_6: calcd for $C_{48}H_{40}F_{24}N_4P_4$, m/z = 1107.2173 $[M - PF_6]^+$, 481.1263 $[M - 2PF_6]^{2+}$; found, 1107.2184 $[M - PF_6]^+$, 481.1278 $[M - 2PF_6]^{2+}$. ^{1}H NMR (500 MHz, CD_3CN, ppm): δ_H 8.78 (AA′ of AA′XX′, J = 7.0 Hz, 8H), 8.18 (XX′ of AA′XX′, J = 6.9 Hz, 8H), 7.93 (s, 8H), 7.61 (s, 8H), 5.68 (s, 8H). ^{13}C NMR (125 MHz, CD_3CN, ppm): δ_C 155.5, 145.1, 137.4, 137.1, 131.1, 130.2, 126.7, 64.8. ^{1}H NMR (500 MHz, CD_3COCD_3, ppm): δ_H 9.28 (AA′ of AA′XX′, J = 7.1 Hz, 8H), 8.51 (XX′ of AA′XX′, J = 7.1 Hz, 8H), 8.15 (s, 8H), 7.86 (s, 8H), 6.08 (s, 8H). ^{13}C NMR (125 MHz, CD_3COCD_3, ppm): δ_C 155.2, 145.5, 137.4, 137.3, 131.3, 130.2, 126.6, 64.7.

Crystal Parameters. ***ExBox·4PF6:*** $[C_{48}H_{40}N_4{\cdot}(PF_6)_4]{\cdot}(MeCN)_3$; colorless block, 0.13 × 0.12 × 0.11 mm; monoclinic, $C2/c$; a =

dx.doi.org/10.1021/ja307360n | J. Am. Chem. Soc. 2013, 135, 183−192

21.920(6), b = 16.300(5), and c = 36.904(11) Å; α = 90.000, β = 98.513(2), and γ = 90.000°; V = 13 040.3(7) Å^3; Z = 8; T = 100(2) K; ρ_{calc} = 1.402 g cm^{-3}; μ = 2.059 mm^{-1}. CCDC no.: 893549.

ExBox⊂Azulene·4PF$_6$(azulene) (1): [$C_{48}H_{40}N_4$⊂$C_{10}H_8$·$(PF_6)_4$]·($C_{10}H_8$)·$(MeCN)_3$; gold block, 0.33 × 0.24 × 0.14 mm; triclinic, $P\bar{1}$; a = 10.090(3), b = 11.382(3), and c = 18.082(5) Å; α = 71.694(10), β = 79.448(10), and γ = 65.810(10)°; V = 1794.77(9) Å^3; Z = 1; T = 100(2) K; ρ_{calc} = 1.510 g cm^{-3}; μ = 1.971 mm^{-1}. CCDC no.: 893550.

ExBox⊂Anthracene·4PF$_6$(anthracene) (2): [$C_{48}H_{40}N_4$⊂$C_{14}H_{10}$·$(PF_6)_4$]·($C_{14}H_{10}$)·$(MeCN)_2$; red block, 0.11 × 0.05 × 0.05 mm; monoclinic, $P2/c$; a = 11.174(3), b = 18.965(5), and c = 33.876(8) Å; α = 90.000, β = 90.818(10), and γ = 90.000°; V = 7177.8(3) Å^3; Z = 4; T = 100(2) K; ρ_{calc} = 1.565 g cm^{-3}; μ = 1.992 mm^{-1}. CCDC no.: 893551.

ExBox⊂Phenanthrene·4PF$_6$(phenanthrene) (3): [$C_{48}H_{40}N_4$⊂$C_{14}H_{10}$·$(PF_6)_4$]·($C_{14}H_{10}$)·$(MeCN)_2$; yellow block, 0.37 × 0.12 × 0.09 mm; monoclinic, $C2/c$, a = 11.247(7), b = 19.121(13), and c = 33.700(2) Å; α = 90.000, β = 90.897(14), and γ = 90.000°; V = 7246(8) Å^3; Z = 4; T = 100(2) K; ρ_{calc} = 1.550 g cm^{-3}; μ = 1.973 mm^{-1}. CCDC no.: 893552.

ExBox⊂Pyrene·4PF$_6$(pyrene) (4): [$C_{48}H_{40}N_4$⊂$C_{16}H_{10}$·$(PF_6)_4$]·($C_{16}H_{10}$)·$(MeCN)_2$; orange block, 0.30 × 0.14 × 0.14 mm; triclinic, $P\bar{1}$; a = 9.926(3), b = 10.725(4), and c = 18.056(6) Å; α = 97.803(10), β = 91.899(10), and γ = 103.705(10)°; V = 1845.73(11) Å^3; Z = 1; T = 100(2) K; ρ_{calc} = 1.565 g cm^{-3}; μ = 1.956 mm^{-1}. CCDC no.: 893553.

ExBox⊂Tetracene·4PF$_6$ (5): [$C_{48}H_{40}N_4$⊂$(C_{16}H_{10})_{0.5}$·$(PF_6)_4$]·$(C_7H_8)_2$·$(MeCN)_2$; red block, 0.47 × 0.16 × 0.07 mm; triclinic, $P\bar{1}$; a = 10.140(3), b = 11.252(3), and c = 17.944(5) Å; α = 72.280(17), β = 86.535(17), and γ = 65.818(15)°; V = 1774.21(9) Å^3; Z = 1; T = 105.4(2) K; ρ_{calc} = 1.529 g cm^{-3}; μ = 1.989 mm^{-1}. CCDC no.: 893554.

ExBox⊂Tetraphene·4PF$_6$ (6): [$C_{48}H_{40}N_4$⊂$(C_{18}H_{12})_{0.5}$·$(PF_6)_4$]·$(MeCN)_3$; orange block, 0.76 × 0.22 × 0.12 mm; triclinic, $P\bar{1}$; a = 10.143(4), b = 11.110(4), and c = 17.953(7) Å; α = 74.054(2), β = 84.440(2), and γ = 64.486(2)°; V = 1754.90(12) Å^3; Z = 1; T = 100(2) K; ρ_{calc} = 1.410 g cm^{-3}; μ = 1.959 mm^{-1}. CCDC no.: 893555.

ExBox⊂Chrysene·4PF$_6$ (7): [$C_{48}H_{40}N_4$⊂$(C_{18}H_{12})$·$(PF_6)_4$]·$(MeCN)_6$; orange block, 0.58 × 0.33 × 0.17 mm; monoclinic, $P2/n$; a = 11.017(5), b = 14.579(7), and c = 24.259(7) Å; α = 90.000, β = 98.998(2), and γ = 90.000°; V = 3848.5(3) Å^3; Z = 2; T = 100(2) K; ρ_{calc} = 1.491 g cm^{-3}; μ = 0.209 mm^{-1}. CCDC no.: 893556.

ExBox⊂[4]Helicene·4PF$_6$ (8): [$C_{48}H_{40}N_4$⊂$(C_{18}H_{12})$·$(PF_6)_4$]·$(MeCN)_2$; yellow block, 0.11 × 0.08 × 0.02 mm; triclinic, $P\bar{1}$; a = 10.561(6), b = 11.101(6), and c = 18.025(11) Å; α = 72.955, β = 82.376(2), and γ = 63.569°; V = 1809.2(18) Å^3; Z = 1; T = 220(2) K; ρ_{calc} = 1.417 g cm^{-3}; μ = 1.918 mm^{-1}. CCDC no.: 893557.

ExBox⊂Triphenylene·4PF$_6$ (9): [$C_{48}H_{40}N_4$⊂$(C_{18}H_{12})$·$(PF_6)_4$]·$(MeCN)_3$; yellow block, 0.35 × 0.21 × 0.04 mm; triclinic, $P\bar{1}$; a = 10.019(12), b = 10.770(13), and c = 18.071(2) Å; α = 73.537(6), β = 74.926(6), and γ = 70.374(4)°; V = 1731.9(4) Å^3; Z = 1; T = 100(2) K; ρ_{calc} = 1.538 g cm^{-3}; μ = 0.224 mm^{-1}. CCDC no.: 893558.

ExBox⊂Perylene·4PF$_6$ (10): [$C_{48}H_{40}N_4$⊂$(C_{20}H_{12})$·$(PF_6)_4$]·$(MeCN)_7$; red block, 0.59 × 0.44 × 0.33 mm; monoclinic, $P2/c$; a = 20.957(5), b = 17.985(5), and c = 22.883(6) Å; α = 90.000, β = 107.919(10), and γ = 90.000°; V = 8206.5(4) Å^3; Z = 4; T = 100(2) K; ρ_{calc} = 1.451 g cm^{-3}; μ = 1.793 mm^{-1}. CCDC no.: 893559.

ExBox⊂Coronene·4PF$_6$ (11): [$C_{48}H_{40}N_4$⊂$(C_{24}H_{12})$·$(PF_6)_4$]·$(MeCN)_7$; orange block, 0.46 × 0.30 × 0.09 mm; triclinic, $P\bar{1}$; a = 10.573(6), b = 14.317(7), and c = 14.733(8) Å; α = 102.508(3), β = 93.376(3), and γ = 109.336(3)°; V = 2033.67(19) Å^3; Z = 1; T = 100(2) K; ρ_{calc} = 1.503 g cm^{-3}; μ = 0.203 mm^{-1}. CCDC no.: 893560.

3. RESULTS AND DISCUSSION

The chemical constitution of the high-affinity PAHs receptor (Scheme 1) is based on the well-known[15] family of π-electron-poor viologen salts, more specifically the phenylene-bridged 4,4′-bipyridines, which are known[16] throughout the literature as "extended viologens". The synthesis begins by treating the extended bipyridine[17] (**ExBIPY**) with an excess of α,α'-dibromo-p-xylene in a refluxing $MeCN/CH_2Cl_2$ solvent mixture (2:1), which initially produces the yellow, water-soluble bromide salt (**DB**·2Br, not shown) after 2 days. In order to render the initial viologen salt soluble in organic media for the next step, the bromide salt is converted to the hexafluorophosphate salt (**DB**·2PF$_6$) by first dissolving **DB**·2Br in MeOH, as opposed to H_2O as a consequence of the poor solubility of **DB**·2Br and potential hydrolysis at the benzylic positions, followed by the addition of solid NH_4PF_6 and subsequent precipitation of **DB**·2PF$_6$ after copious amounts of H_2O is added (approximately a few liters for every 500 mL of MeOH used). In the final step, two synthetic pathways lead to the final viologen-based tetracationic cyclophane (**ExBox**·4PF$_6$). The first pathway consists of simply mixing **DB**·2PF$_6$ and **ExBIPY** in a 1:1 ratio in MeCN and allowing the reaction to proceed for a little over 2 weeks. The yield from this reaction, however, is low (19%). Therefore, a method involving templation[18] was adopted wherein 3 equiv of pyrene is used to help stabilize the transition state during cyclophane closure as a result of donor−acceptor interactions between the π-electron-rich pyrene and the π-electron-poor extended viologen units of **ExBox**$^{4+}$. Moreover, the pyrene template is removed easily by solvent extraction with CH_2Cl_2, which changes the organic layer from an orange solution to a white suspension, after the desired cyclophane has been converted to the chloride salt (**ExBox**·4Cl, not shown). The final step of the synthesis involves another counterion exchange wherein the chloride salt (**ExBox**·4Cl) is converted to the hexafluorophosphate salt by adding solid NH_4PF_6, an action which precipitates white **ExBox**·4PF$_6$ from the water layer. This method affords the desired product in 42% yield after silica column chromatography, 1% NH_4PF_6 in MeCN (w/v), and several recrystallizations. A more detailed synthetic procedure and spectroscopic analysis of each compound can be found in the SI.

From a photophysical perspective, **ExBox**$^{4+}$ demonstrates (Figure 2a) a strong absorbance in the ultraviolet region at 319 nm. Upon addition of a π-electron-rich guest and formation of a 1:1 complex (**ExBox**$^{4+}$⊂guest), the optical absorption data show (Figure S13) the emergence of a charge-transfer band (400−650 nm) in the visible region of the spectrum. All of the electron-donating guests assessed (Figure 1), with the exception of azulene and tetracene, exhibit this behavior. In the case of the former, there appears to be no change in the absorption spectra (Figure S13a) when **ExBox**$^{4+}$ is mixed with azulene in a 1:1 ratio, as compared to the superposition of the individual molecular spectra. No absorption data were obtained for the **ExBox**$^{4+}$⊂tetracene inclusion complex because of solubility issues associated with tetracene. It is important to note that the **ExBox**⊂tetracene·4PF$_6$ single crystals (**5**), shown in Figure 1, were obtained by first heating the 1:1 mixture of the π-electron-rich guest and **ExBox**$^{4+}$ in PhMe/MeCN (1:1) prior to dilution with an additional MeCN and crystallization.

Analysis of the cyclic voltammogram (CV, Figure 2b) of **ExBox**$^{4+}$ and the phenylene-bridged methyl viologen (**MPV**$^{2+}$) provides some insight into the electrochemical behavior of the extended viologen units on an individual basis as well as when more than one unit is part of a rigid cyclophane. The CV (blue trace, Figure 2b) of **MPV**$^{2+}$ consists essentially of one broad redox couple where the two one-electron reduction waves overlap completely at −0.82 V, an observation which is an

dx.doi.org/10.1021/ja307360n | J. Am. Chem. Soc. 2013, 135, 183−192

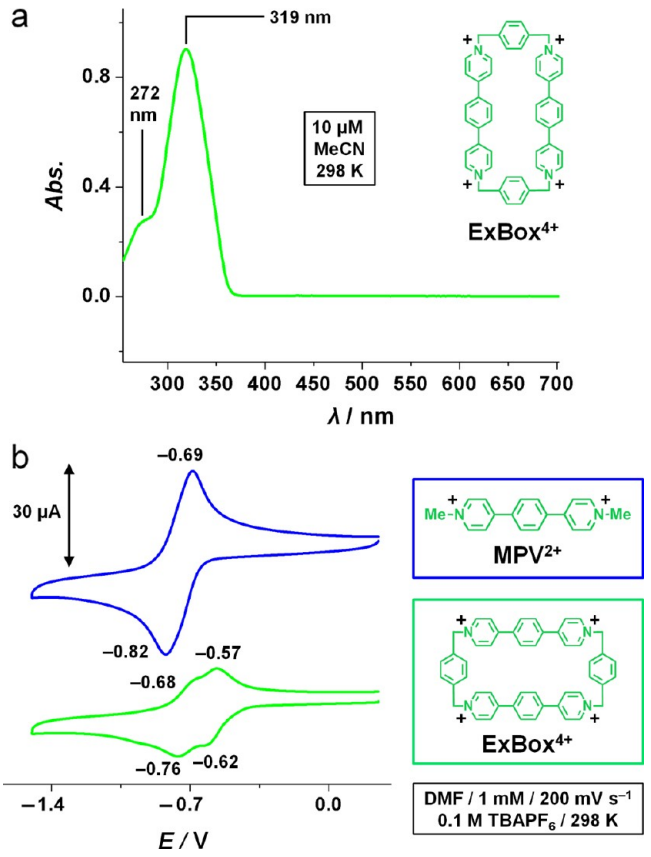

Figure 2. UV/vis absorption spectrum (a) of **ExBox**$^{4+}$ displaying a strong absorbance band centered around 319 nm and sharing no bands in the visible region. The CV (b) of the phenylene-bridged methyl viologen (MPV^{2+}) shows one broad redox couple, which consists of two one-electron redox processes and occurs as a result of a lack of communication between the two redox centers of the molecule. In contrast, the CV of **ExBox**$^{4+}$ demonstrates a splitting of the two redox couples (by 140 mV), presumably a consequence of the steric and electronic constraints associated with the rigid geometry of the cyclophane. A glassy carbon working electrode, a platinum counter electrode, and a Ag/AgCl reference electrode were used to characterize a 1 mM DMF solution of **ExBox**$^{4+}$ at 298 K with 0.1 M $TBAPF_6$ serving as the electrolyte. A scan rate of 200 mV s^{-1} was used for this analysis.

indication that the two bipyridinium redox centers are not communicating[19] and behave quite independently of one another. Conversely, the CV of **ExBox**$^{4+}$ consists of two closely overlapping two-electron redox couples, where the potentials of the two cathodic peaks are separated by 140 mV. This separation reflects the level of electronic communication between the two redox centers of each extended bipyridinium unit insofar as that, after formation of the radical cationic **ExBox**$^{2(\bullet+)}$, the second two-electron reduction, which leads to the formation of the neutral species, is shifted to lower potentials and is therefore more difficult to reduce. This direct comparison demonstrates how the electronic properties of the extended viologen units can be altered by controlling the steric and electronic environment as well as incorporating them into a rigid cyclophane.

Figure 1 illustrates the superstructures of host−guest complexes of **ExBox**$^{4+}$ with 11 PAH guests viewed from different angles, as obtained from the XRD analysis of single crystals of these complexes. They demonstrate the remarkable ability of **ExBox**$^{4+}$ to scavenge a large number of PAHs varying in size (from azulene up to coronene) and shape (from linear tetracene to star-like triphenylene). Looking at the manner in which the locally flexible, yet globally rigid **ExBox**$^{4+}$ cyclophane adapts to different guests by adopting small and subtle changes in its conformation, one senses that the pool of PAH molecules that can be bound inside **ExBox**$^{4+}$ is not limited only to these 11 examples but, most likely, many more—potentially harmful—smaller PAHs can be trapped inside this promiscuous receptor.

High-quality single crystals of **ExBox**$^{4+}$ and its inclusion complexes were obtained by slow vapor diffusion of $i\mathrm{Pr}_2\mathrm{O}$ into the solution of **ExBox**$^{4+}$ and the 1:1.1 stoichiometric mixtures of **ExBox**$^{4+}$ with the PAHs in MeCN over a period of a few days. The color of these crystals (Figure 1) corresponds to the absorption wavelength of the charge-transfer band of the corresponding complex in solution (see the SI) and makes it possible for one to detect visually when a PAH molecule binds inside **ExBox**$^{4+}$. This feature makes **ExBox**$^{4+}$ a suitable candidate for visual PAH sensing.

The dimensions of the cavity of **ExBox**$^{4+}$ are 6.9 Å (width) × 14.6 Å (length) as deduced from the distances between the aromatic planes on opposite sides of the empty cyclophane in the X-ray crystal structure (see the SI) and approximately 3.5 Å (width) × 11.2 Å (length) when considering the van der Waals radii. The 6.9 Å value is similar to that reported for an analogous tetracationic cyclophane, cyclobis(paraquat-*p*-phenylene)[20] (**CBPQT**$^{4+}$), which is known to bind smaller aromatic guests by means of donor−acceptor charge-transfer interactions, where the typical dihydroxynaphthalene-derived guests reside in the **CBPQT**$^{4+}$ ring in a perpendicular manner.[18] Both **CBPQT**$^{4+}$ and **ExBox**$^{4+}$ bind π-electron-rich guests effectively as a result of their inherent $\pi-\pi$ stacking distances (3.5 Å) between the π-electron-poor units of the host and the guest. The ability of **ExBox**$^{4+}$ to bind larger PAH guests relative to **CBPQT**$^{4+}$ is a consequence of the inside length parameter of **ExBox**$^{4+}$ (approximately 7.8 Å). Coronene is the largest guest (in one dimension) we have investgated. In principle, thin graphene nanoribbons that would be "coronene-wide" in one dimension (i.e., approximately 7.3 Å) could potentially serve as a guest for multiple host molecules of **ExBox**$^{4+}$.

The general trend, which becomes evident when comparing the crystal superstructures of **1**−**11**, is that each PAH guest adopts the greatest possible $\pi-\pi$ overlap with the extended bipyridinium (**ExBIPY**$^{2+}$) units of **ExBox**$^{4+}$. This principle can be demonstrated quite nicely by comparing the two linear PAH molecules, anthracene and tetracene. While the shorter anthracene (7.3 Å) is fully aligned inside **ExBox**$^{4+}$, the length of tetracene (9.7 Å) overcomes the size limit of **ExBox**$^{4+}$ and is forced out of colinearity by approximately 44°, and the two terminal benzenoid rings protrude outside the cavity (Figure 1). Also, as the size of the PAH guest is increased, the torsion angles between the pyridinium and the phenylene rings of **ExBox**$^{4+}$ tend to decrease, reaching a lower limit in the case of perylene.

The size and shape of the PAH guests play an important role also on the overall packing (Figure 5 and the SI) in the crystal. Generally, the smaller PAHs (**1**−**4**) crystallize in a 2:1 (PAH:**ExBox**$^{4+}$) manner, where one PAH molecule binds inside **ExBox**$^{4+}$ and the second molecule is located in the outer space interacting through C−H···π interactions with **ExBox**$^{4+}$ or the complexed PAH molecules, while the larger PAHs (**7**−**11**) crystallize in a 1:1 (PAH:**ExBox**$^{4+}$) fashion, where all of the

dx.doi.org/10.1021/ja307360n | J. Am. Chem. Soc. 2013, 135, 183−192

Table 1. Binding Parameters and H_γ-Proton Shifts of the Studied 1:1 ExBox^{4+}⊂PAH Complexes 1−11

		binding parameters				
1:1 complex	π-electron count[a]	$K_a/10^3$ (M^{-1})	ΔH (kcal mol^{-1})	ΔS (cal mol^{-1} K^{-1})	ΔG (kcal mol^{-1})	δ (ppm)[b]
1	10	0.286 ± 0.011[c]	–	–	−3.35 ± 0.022	7.86
2	14	0.883 ± 0.11[c]	–	–	−4.01 ± 0.073	7.38
3	14	1.38 ± 0.016[d]	−5.72 ± 0.024	−4.83 ± 0.084	−4.28 ± 0. 0068	7.26
4	16	7.16 ± 0.50[d,e]	−5.84 ± 0.076	−1.97 ± 0.29	−5.25 ± 0.041	6.76
5	18	–[f]	–	–	–	–[g]
6	18	0.914 ± 0.010[d]	−5.79 ± 0.028	−5.91 ± 0.096	−4.03 ± 0.0065	7.19
7	18	2.32 ± 0.15[c]	–	–	−4.59 ± 0.038	7.10
8	18	5.71 ± 0.054[d]	−7.66 ± 0.018	−8.52 ± 0.063	−5.12 ± 0.0056	6.93
9	18	19.7 ± 5.0[c]	–	–	−5.85 ± 0.15	6.91
10	20	88.1 ± 67[c]	–	–	−6.74 ± 0.45	6.90
11	24	–[f]	–	–	–	5.40

[a]Number of π-electrons in the PAH aromatic system. [b]Chemical shifts of the H_γ-protons of the 1:1 complex. [c]Determined by ^{1}H NMR spectroscopy. [d]Determined by ITC. [e]Binding constant determined by ^{1}H NMR spectroscopy for complex **4** is 10.1 ± 1.1 × 10^3 M^{-1}. [f]Binding parameters of these complexes could not be determined by either ITC or NMR spectroscopy on account of solubility restrictions. [g]Chemical shift of the H_γ-protons of this complex could not be determined because of solubility restrictions.

PAH molecules are inside **ExBox**$^{4+}$. The two exceptions (**5** and **6**) to this experimental observation, which are, sizewise, somewhere in between the smaller and larger studied PAHs, crystallize in a 1:2 (PAH:**ExBox**$^{4+}$) manner; half of the **ExBox**$^{4+}$ hosts in the superstructure being empty. This phenomenon could play an important role in the tuning of the overall properties of such "superstacks" when considering their possible functions as organic semiconductors. Additionally, a certain degree of disorder of PAH molecules, either inside or outside of **ExBox**$^{4+}$ or both, in the superstructure was observed in some cases (**1**, **3**, **5**, **6**, **8**, and **9**; see the SI).

It should be noted that the least planar guest [4]helicene possesses a twisted helical conformation, demonstrating the ability of **ExBox**$^{4+}$ to bind PAHs is not strictly limited to the planar guests. The high-affinity diverse binding capability of **ExBox**$^{4+}$ arises, presumably, from the locally flexible character of this globally rigid cyclophane.

The thermodynamic parameters (ΔH, ΔS, and ΔG) and the association constants (K_a) for the 1:1 complexes of **ExBox**$^{4+}$ with PAH guests (**1**−**11**) in solution (MeCN) are summarized in Table 1. The thermodynamic parameters for the binding events of **ExBox**$^{4+}$ with the PAHs (complexes **3**, **4**, **6**, and **8**) were obtained by ITC in dry, degassed MeCN at 298 K. The restricted solubility of the remainder (complexes **1**, **2**, **5**, **7**, and **9**−**11**) of the PAHs in MeCN prohibited us from using ITC to monitor the thermodynamic parameters of binding. ^{1}H NMR spectroscopy was used to obtain K_a values for the association between **ExBox**$^{4+}$ and the PAHs which are, at least partially, soluble in $CDCl_3$ (complexes **1**, **2**, **7**, **9**, and **10**). In the case of complexes **5** and **11**, the extremely low solubility of tetracene and coronene, respectively, in most organic solvents render it impossible for us to obtain K_a values for these complexes. Details on both methods and determination of the binding parameters are provided in the SI.

Comparison of the full thermodynamic parameters available for the four complexes **3**, **4**, **6**, and **8** leads to the conclusion that the host−guest binding process is mainly enthalpy driven in the case of **3**, **6**, and **8**. With **4**, however, a surprisingly small change in entropy (ΔS), which contributes to the large K_a value for this complex, was observed. Although the complexes of **ExBox**$^{4+}$ with **4** and **6** have very similar values of ΔH, the K_a values for the complex with **6** differs by approximately a factor of 7 compared with that for **4**. This low value of ΔS in the case of **4** could be caused by the presence[21] of dimeric forms of pyrene in MeCN, decreasing the entropy of the initial (prior-to-complexation) state.

The ^{1}H NMR spectra (Figure 3 and the SI) of the 1:1 **ExBox**$^{4+}$⊂PAH complexes display significant upfield shifts for the signals corresponding to β and γ protons of **ExBox**$^{4+}$ and all of the signals for the protons of the PAH guests as well as a downfield shift of the phenylene protons of **ExBox**$^{4+}$. This pattern is caused by π-electron shielding of the face-to-face oriented aromatic rings, which occurs upon complexation. The α and CH_2 protons of **ExBox**$^{4+}$ display only very slight shifts in their ^{1}H NMR spectra since they are located in the "corners" of **ExBox**$^{4+}$ and are therefore not affected significantly by the shielding effect of PAH guests. This behavior is in excellent agreement with the inclusion of PAH guests inside **ExBox**$^{4+}$ in the solution state. Additionally, it is important to note that there are only one set of proton signals observed for **ExBox**$^{4+}$ and the guest, as a result of the various species that exist in equilibrium undergoing fast exchange on the ^{1}H NMR time scale.

A general trend associated with the binding affinity of **ExBox**$^{4+}$ toward PAH guests exists, whereby the stability constant of the complex increases exponentially (Figure 4a) as the PAH guests become more π-electron-rich resulting in greater π−π interactions between the host and guest. This trend is exhibited by all of the complexes, except for **6**−**8**, which cannot adopt maximum π−π overlap on account of the unfavorable size/shape of the PAH guest. The side-on view (Figure 1) of the crystal superstructure of **6**−**9** reveals that the face-to-face π−π overlaps between **ExBox**$^{4+}$ and the PAH molecules increase with higher and higher K_a values. A similar (although linear) trend is observed (Figure 4b) when the difference between the chemical shifts (in ppm) of the γ protons of the 1:1 complexes and those for the unbound **ExBox**$^{4+}$ is plotted against the number of π-electrons in the PAH molecule. In this case, the chemical shift not only depends on the K_a value, which correlates to the number of π-electrons, but also directly on the number of π-electrons as they dictate the shielding effect of the PAH guest.

Four PAH guests (varying between three and seven rings) were explored (Figure 5) in a solid-state setting on SiO_2 platforms in the form of 2:1 or 1:1 inclusion complexes with **ExBox**$^{4+}$. By lowering the concentration of the host and guest

dx.doi.org/10.1021/ja307360n | J. Am. Chem. Soc. 2013, 135, 183−192

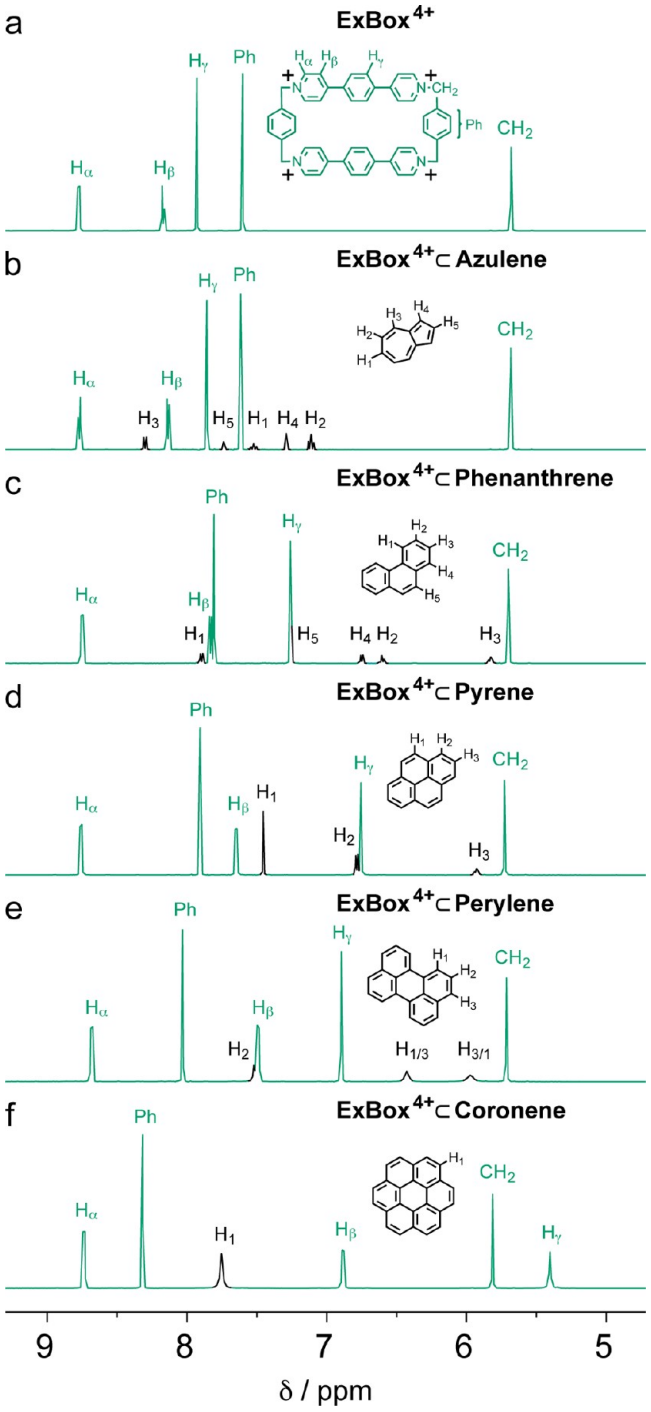

Figure 3. Aromatic-region insets of the ^{1}H NMR spectra of **ExBox**⊂4PF$_6$ (a) and its 1:1 complexes with azulene (b), phenanthrene (c), pyrene (d), perylene (e), and coronene (f) recorded in CD_3CN at 298 K on a 500 MHz instrument. Upfield shifts of the β and γ protons of **ExBox**$^{4+}$ as well as downfield shifts of the phenylene protons of **ExBox**$^{4+}$ are evident. Both downfield and upfield shifts increase as the size of the PAH core becomes larger and larger, indicating the binding of a PAH molecule inside **ExBox**$^{4+}$ in solution.

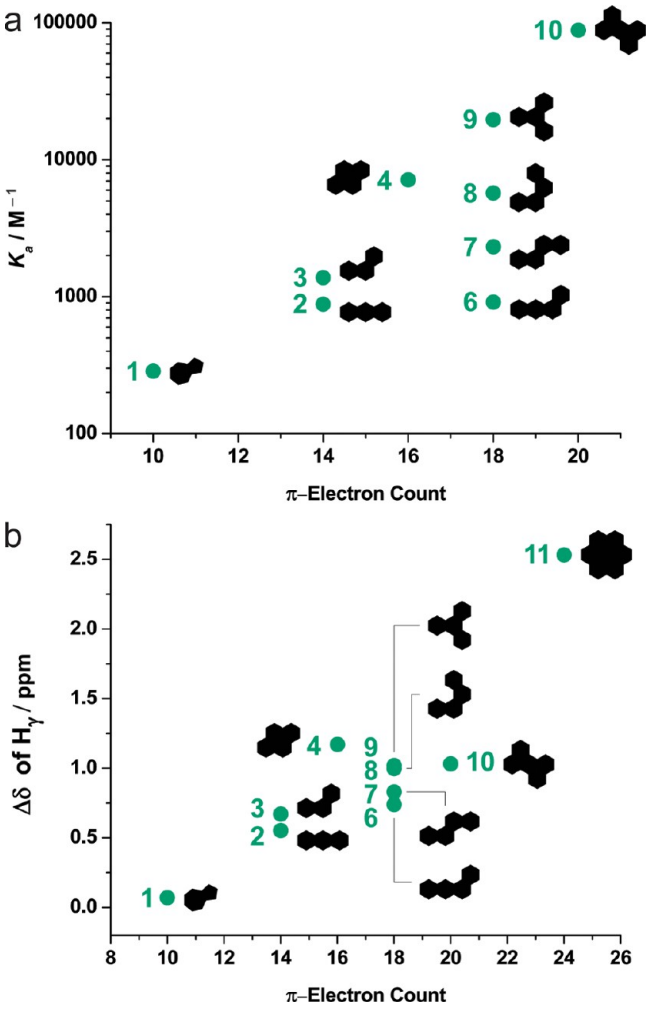

Figure 4. K_a values (a) and chemical shift differences of the γ protons of **ExBox**$^{4+}$ (7.93 ppm) and its 1:1 complex ($\Delta\delta$ of H$_\gamma$) (b) plotted against the number of π-electrons present in the respective PAH. Both K_a (exponential behavior; logarithmic scale was used for the y-axis) and $\Delta\delta$ values for H$_\gamma$ (linear behavior) increase as the number of π-electrons becomes larger and larger and show that the binding affinity of **ExBox**$^{4+}$ toward PAHs is related directly to the increase of the size of the PAH core.

to 0.625 and 0.750 mM in MeCN, respectively, micrometer-sized single crystals were obtained for **ExBox**⊂anthracene·4PF$_6$(anthracene) (three rings, Figure 5a), **ExBox**⊂pyrene·4PF$_6$(pyrene) (four rings, Figure 5b), **ExBox**⊂perylene·4PF$_6$ (five rings, Figure 5c), and **ExBox**⊂coronene·4PF$_6$ (seven rings, Figure 5d). Their scanning electron microscopy (SEM) images, displayed in Figure 5, provide a sense of the crystal morphology of each of the complexes that were grown on the SiO_2 surface. The superstructures of each complex, shown to the right of each SEM image in Figure 5, demonstrate the packing of the individual inclusion complexes. In the case of anthracene (Figure 5a) and pyrene (Figure 5b), the molecules are ordered in an alternating fashion, whereby the inclusion complexes are intercalated with continuous sheets of the electron-rich PAHs, a feature which could lead potentially to these materials functioning in an organic field-effect transistor. In the perylene (Figure 5c) and coronene (Figure 5d) superstructures, however, the individual complexes do not appear to pack into discrete donor–acceptor domains but instead are organized through intermolecular steric interactions between each complex.

In order to demonstrate the high affinity that **ExBox**$^{4+}$ has for PAHs in a mixture of hydrocarbons, a crude oil sample from Saudi Arabia containing an unspecified array of aromatic compounds was tested against **ExBox**·4Cl in water. The results

dx.doi.org/10.1021/ja307360n | J. Am. Chem. Soc. 2013, 135, 183–192

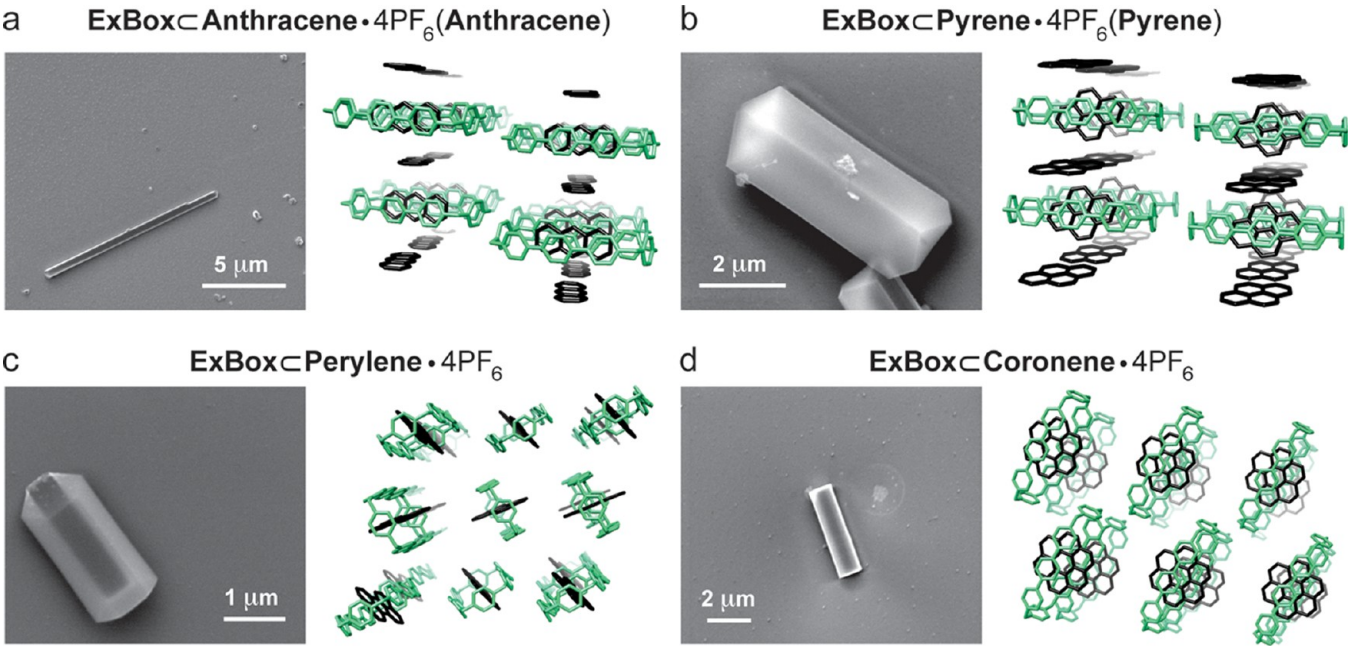

Figure 5. SEM images of the single crystals of the four inclusion complexes **ExBox**⊂anthracene·4PF_6(anthracene) (a), **ExBox**⊂pyrene·4PF_6(pyrene) (b), **ExBox**⊂perylene·4PF_6 (c), and **ExBox**⊂coronene·4PF_6 (d) showing the micrometer-sized crystals that formed on SiO_2 wafers after drop-casting mixed solutions of host and guest (0.625 and 0.750 mM, respectively) in MeCN onto the surface and carrying out slow vapor diffusion using *i*PrO_2 over the course of 1−3 days. The superstructures to the right of each SEM image were generated from X-ray crystallography carried out on single crystals that were grown at a higher concentration (3.0 mM) and used to obtain the single-crystal XRD data shown in Figure 1. In the case of the superstructures where a smaller guest was employed, i.e., three and four rings, it should be noted that the sheets of inclusion complexes are separated by sheets of the free guest (a,b), whereas in the case of the larger guests, the packing in the crystal consists of only the 1:1 inclusion complexes and no intercalated PAHs are observed (c,d). The PF_6^- counterions and the solvent molecules in the superstructures are omitted for clarity.

of this investigation are summarized in Figure 6. The starting crude oil mixture (Figure 6a) was first diluted (i) with CD_2Cl_2 (150 μL of oil added to 4 mL) before the addition (ii) of **ExBox**·4Cl in 4 mL of D_2O (8 mM) on top of the oil, taking care not to disturb the oily layer. The vial labeled "6-C" in Figure 6a is the control mixture where 4 mL of D_2O only was added to the oily layer, and it was later found to contain no PAHs. After shaking the oil−water mixture (which contains $\mathbf{ExBox}^{4+}$) by hand for approximately 2 min (iii), the color of the aqueous phase turned to an orange-yellow hue, which is different from the previous lighter-colored suspension before the two phases had been mixed. After separation of the two phases, the aqueous layer was siphoned off and the newly acquired aromatic guests were isolated (iv) by solvent extraction using a few iterations of CH_2Cl_2, while simultaneously regenerating the $\mathbf{ExBox}^{4+}$ in aqueous solution. Figure 6a (far right) shows the final isolated PAHs (1.2 mg from 150 μL of crude oil) after CH_2Cl_2 had been evaporated. ^{1}H NMR spectra recorded at each stage of the PAHs isolation procedure are presented in Figure 6b. The spectrum at the top of Figure 6b shows ^{1}H NMR peaks in the aromatic region present in the starting oily layer. The ^{1}H NMR spectrum directly below the crude oil spectrum shows that $\mathbf{ExBox}^{4+}$ has been successful in extracting a range of different aromatic hydrocarbons in the crude oil. The ^{1}H NMR spectrum of $\mathbf{ExBox}^{4+}$ before the two phases were mixed shows the starting chemical shifts of each proton in the aromatic region in D_2O, whereas the spectrum recorded after extraction of aromatics from the crude oil solution shows small changes in the chemical shifts of the α, β, and phenylene protons and a more dramatic shifting of the resonances for the γ protons. In an effort to characterize the extracted aromatic compounds, GC-MS studies were conducted on four standards (*trans*-stilbene, phenanthrene, anthracene, and pyrene; Figure 6c) as well as the mixture of aromatic compounds that were extracted from the crude oil in steps iii and iv. This general MS characterization makes it possible to generate mass ranges and molecular formulas for the extracted aromatic material and gives a sense of the sizes of compounds $\mathbf{ExBox}^{4+}$ is capable of scavenging. Overall, the oil extraction study demonstrates clearly the ability of $\mathbf{ExBox}^{4+}$ to pull out potentially harmful PAHs from a crude mixture of oil, which contains a large number of different aromatic hydrocarbons.

4. CONCLUSIONS

In summary, we have reported the synthesis and full characterization of a robust tetracationic organic cyclophane, $\mathbf{ExBox}^{4+}$, which serves as a promiscuous high-affinity PAH scavenger in both organic and aqueous media. This PAH receptor was obtained starting from easily accessible precursors using pyrene to template the cyclophane-closing step, affording ultimately **ExBox**·4PF_6 in 42% yield. In order to demonstrate the high flexibility of $\mathbf{ExBox}^{4+}$ to bind practically any small—potentially harmful—PAHs, 11 representative PAHs, ranging in size from two to seven fused aromatic rings, were trapped inside $\mathbf{ExBox}^{4+}$, and the resulting complexes were fully characterized, including the single-crystal superstructure determinations of all 11 of them. Considering the known harmful effects of many of the smaller PAHs on the environment and people, we envisage that this $\mathbf{ExBox}^{4+}$ PAH scavenger will play a key role in the extraction and detection of harmful PAHs from the environment as well as in the purification processes relating to both water and crude oil. Furthermore, the well-defined donor−acceptor superstacks of

dx.doi.org/10.1021/ja307360n | *J. Am. Chem. Soc.* 2013, 135, 183−192

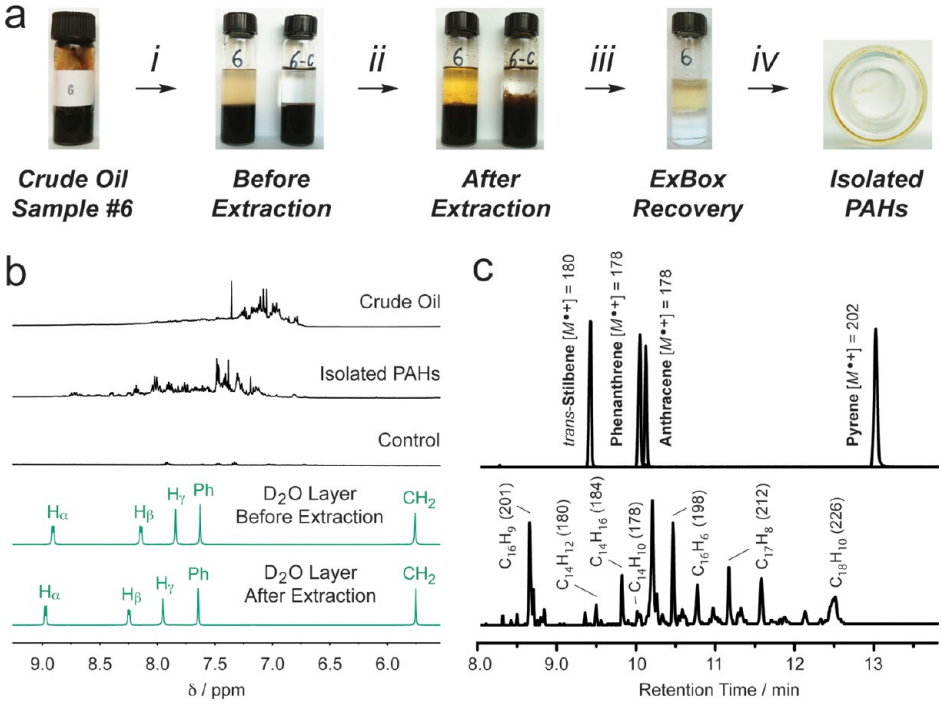

Figure 6. (a) A crude oil sample ("6") from Saudi Arabia, containing an unknown amount of unspecified aromatic compounds, was first (i) diluted with CD_2Cl_2 (150 μL of oil added to 4 mL) and subsequently (ii) extracted with a solution of **ExBox**·4Cl in D_2O (8.0 mM, 4 mL) (intensive shaking of the mixture for approximately 2 min), upon which the aqueous phase turned to an orange-yellow hue indicating supramolecular trapping of PAHs inside **ExBox**$^{4+}$. The orange-yellow solution was then (iii) extracted 3× with CH_2Cl_2 (4 mL each time), and upon (iv) removal of the solvent, the crude-oil extract was analyzed by ^{1}H NMR spectroscopy and found to contain aromatic compounds. The same oil extraction experiment was carried out using a blank (control; "6-C") solution of D_2O without **ExBox**·4Cl, which did not undergo a color change upon extraction (ii) and did not contain any aromatic species (control; ^{1}H NMR in CD_2Cl_2). (b) ^{1}H NMR spectra (in order from top to bottom) for the crude oil sample (in CD_2Cl_2), crude oil extract (in CD_2Cl_2), the control experiment (in CD_2Cl_2), and **ExBox**·4Cl before and after the extraction (both in D_2O), recorded at 298 K on a 500 MHz instrument. (c) GC-MS data for four PAH standards (top) and compared to the material (bottom) extracted from the crude oil in steps iii and iv. From the MS data, it is possible to generate molecular formulas, corresponding to various PAH derivatives that fall within the mass range of the tested standards.

ExBox^{4+} and PAHs, with potential semiconducting properties, could serve as new alternative composite materials in organic field-effect transistors.

■ ASSOCIATED CONTENT

Ⓢ Supporting Information

Detailed synthetic procedures and characterization (NMR and HRMS) data for all compounds, crystallographic and spectroscopic (NMR, UV/vis) characterization for **ExBox**·4PF_6 and inclusion complexes **1**−**11**, ITC data for **3**, **4**, **6**, and **8**. This material is available free of charge via the Internet at http://pubs.acs.org.

■ AUTHOR INFORMATION

Corresponding Author

stoddart@northwestern.edu

Author Contributions

‡These authors contributed equally.

Notes

The authors declare no competing financial interest.

■ ACKNOWLEDGMENTS

Data are tabulated, and the crystallographic parameters of each single crystal were deposited into the Cambridge Crystallographic Data Centre (CCDC). We thank Anastasiya Vinokur for her help with solving and refining the crystal structure of complex **2**. J.F.S. is supported by the Non-Equilibrium Energy Research Center (NERC), which is an Energy Frontier Research Center (EFRC) funded by the U.S. Department of Energy, Office of Basic Energy Sciences (DOE-BES) under award DESC0000989. J.C.B. is supported by a National Defense Science and Engineering Graduate (NDSEG) Fellowship from the Department of Defense (DOD) and gratefully acknowledges support from the Ryan Fellowship awarded under the auspices of the Northwestern University International Institute for Nanotechnology. M.J. is supported by The Netherlands Organisation for Scientific Research (NWO) and the Marie Curie Cofund Action (Rubicon Fellowship). N.L.S. is supported by a Graduate Research Fellowship (GRF) from the National Science Foundation (NSF). P.L.M. acknowledges the NSF and the Georgia Tech Facilitating Academic Careers in Engineering and Science (FACES) committee for a postdoctoral fellowship. C.J.B. is supported by a GRF from the NSF.

■ REFERENCES

(1) Radziszewski, B. *Ber. Dtsch. Chem. Ges.* **1876**, *9*, 260−262.
(2) Simpson, C. D.; Brand, J. D.; Berresheim, A. J.; Przybilla, L.; Räder, H. J.; Müllen, K. *Chem.−Eur. J.* **2002**, *8*, 1424−1429.
(3) (a) Clar, E. *Polycyclic Hydrocarbons*; Academic Press: London, 1964; Vols. *1*−*2*. (b) Clar, E. *The Aromatic Sextet*; John Wiley & Sons: London, 1972. (c) Harvey, R. G. *Polycyclic Aromatic Hydrocarbons*; Wiley-VCH: New York, 1997.
(4) (a) Vijh, U. P.; Witt, A. N.; Gordon, K. D. *Astrophys. J.* **2005**, *619*, 368−378. (b) Vijh, U. P.; Witt, A. N.; Gordon, K. D. *Astrophys. J.* **2004**, *606*, L65−L68.

(5) (a) Tang, J.; Carroquino, M. J.; Robertson, B. K.; Alexander, M. *Environ. Sci. Technol.* **1998**, *32*, 3586−3590. (b) Ghosh, U.; Gillette, J. S.; Luthy, R. G.; Zare, R. N. *Environ. Sci. Technol.* **2000**, *34*, 1729−1736. (c) Boström, C.-E.; Gerde, P.; Hanberg, A.; Jernström, B.; Johansson, C.; Kyrklund, T.; Rannug, A.; Tornqvist, M.; Victorin, K.; Westerholm, R. *Environ. Health Perspect.* **2002**, *110*, 451−488. (d) Werner, D.; Higgins, C. P.; Luthy, R. G. *Water Res.* **2005**, *39*, 2105−2113.

(6) (a) Watson, M. D.; Fechtenkötter, A.; Müllen, K. *Chem. Rev.* **2001**, *101*, 1267−1300. (b) Watanabe, M.; Chang, Y. J.; Liu, S.-W.; Chao, T.-H.; Goto, K.; Islam, M. M.; Yuan, C.-H.; Tao, Y.-T.; Shinmyozu, T.; Chow, T. *Nat. Chem.* **2012**, *4*, 574−578. (c) Rieger, R.; Müllen, K. *J. Phys. Org. Chem.* **2010**, *23*, 315−325.

(7) Marinov, N. M.; Pitz, W. J.; Westbrook, C. K.; Castaldi, M. J.; Senkan, S. M. *Combust. Sci. Technol.* **1996**, *116*, 211−287.

(8) Luch, A. *The Carcinogenic Effects of Polycyclic Aromatic Hydrocarbons*; Imperial College Press: London, 2005.

(9) Scientific Opinion of the Panel on Contaminants in the Food Chain on a request from the European Commission on Polycyclic Aromatic Hydrocarbons in Food. *EFSA J.* **2008**, *724*, 1−114.

(10) (a) Lehn, J.-M. *Supramolecular Chemistry Concepts and Perspectives*; Wiley-VCH: Weinheim, Germany, 1995. (b) Beer, P. D.; Gale, P. A.; Smith, D. K. *Supramolecular Chemistry*; Oxford University Press: Oxford, U.K., 1999. (c) Steed, J. W.; Atwood, J. L. *Supramolecular Chemistry*; Wiley-VCH: Weinheim, Germany, 2009. (d) Stoddart, J. F. *Nat. Chem.* **2009**, *1*, 14−15.

(11) (a) Blyshak, L. A.; Dodson, K. Y.; Patonay, G.; Warner, I. M. *Anal. Chem.* **1989**, *61*, 955−960. (b) Mohseni, R. M.; Hurtubise, R. J. *J. Chromatogr., A* **1990**, *499*, 395−410. (c) Lamparczyk, H.; Zarzycki, P.; Ochocka, R. J.; Sybilska, D. *Chromatographia* **1990**, *30*, 91−94. (d) Butterfield, M. T.; Agbaria, R. A.; Warner, I. M. *Anal. Chem.* **1996**, *68*, 1187−1190. (e) Shixiang, G.; Liansheng, W.; Qingguo, H.; Sukui, H. *Chemosphere* **1998**, *37*, 1299−1305. (f) Ravelet, C.; Ravel, A.; Grosset, C.; Villet, A.; Geze, A.; Wouessidjewe, D.; Peyrin, E. *J. Liq. Chromatogr. Relat. Technol.* **2002**, *25*, 421−432.

(12) (a) Li, H.; Qu, F. *J. Mater. Chem.* **2007**, *17*, 3536−3544. (b) Yin, J.; Wang, L.; Wei, X.; Yang, G.; Wang, H. *J. Chromatogr., A* **2008**, *1188*, 199−207. (c) Bandela, A.; Chinta, J. P.; Hinge, V. K.; Dikundwar, A. G.; Row, T. N. G.; Rao, C. P. *J. Org. Chem.* **2011**, *76*, 1742−1750.

(13) Chen, Y.; Luo, J.; Zhu, X. X. *J. Phys. Chem. B* **2008**, *112*, 3402−3409.

(14) (a) Peinador, C.; Pía, E.; Blanco, V.; García, M. D.; Quintela, J. M. *Org. Lett.* **2010**, *12*, 1380−1383. (b) Blanco, V.; García, M. D.; Terenzi, A.; Pía, E.; Fernández-Mato, A.; Peinador, C.; Quintela, J. M. *Chem.−Eur. J.* **2010**, *16*, 12373−12380.

(15) (a) Michaelis, L.; Hill, E. S. *J. Gen. Physiol.* **1933**, *16*, 859−873. (b) Bird, C. L.; Kuhn, A. T. *Chem. Soc. Rev.* **1981**, *10*, 49−82. (c) Monk, P. M. S. *The Viologens: Physicochemical Properties, Synthesis and Applications of the Salts of 4,4′-Bipyridine*; Wiley: New York, 1998.

(16) (a) Takahashi, K.; Nihira, T.; Akiyama, K.; Ikegami, Y.; Fukuyo, E. *J. Chem. Soc., Chem. Commun.* **1992**, 620−622. (b) Porter, W. W.; Vaid, T. P.; Rheingold, A. L. *J. Am. Chem. Soc.* **2005**, *127*, 16559−16566. (c) Kolivoška, V.; Gál, M.; Pospíšil, L.; Valášek, M.; Hromadová, M. *Phys. Chem. Chem. Phys.* **2011**, *13*, 11422−11429.

(17) Su, Y.-S.; Chen, C. F. *Org. Lett.* **2010**, *12*, 1888−1891.

(18) (a) Brown, C. L.; Philp, D.; Stoddart, J. F. *Synlett* **1991**, *7*, 462−464. (b) Jäger, R.; Vögtle, F. *Angew. Chem., Int. Ed. Engl.* **1997**, *36*, 930−944. (c) Aricó, F.; Badjic, J. D.; Cantrill, S. J.; Flood, A. H.; Leung, K. C.-F.; Liu, Y.; Stoddart, J. F. *Top. Curr. Chem.* **2005**, *249*, 203−259. (d) Dichtel, W. R.; Miljanić, O. Š.; Spruell, J. M.; Heath, J. R.; Stoddart, J. F. *J. Am. Chem. Soc.* **2006**, *128*, 10388−10390. (e) Stoddart, J. F. *Chem. Soc. Rev.* **2009**, *38*, 1802−1820.

(19) Flanagan, J. B.; Margel, S.; Bard, A. J.; Anson, F. C. *J. Am. Chem. Soc.* **1978**, *100*, 4248−4253.

(20) (a) Odell, B.; Reddington, M. V.; Slawin, A. M. Z.; Spencer, N.; Stoddart, J. F.; Williams, D. J. *Angew. Chem., Int. Ed. Engl.* **1988**, *27*, 1547−1550. (b) Asakawa, M.; Dehaen, W.; L'abbé, G.; Menzer, S.; Nouwen, J.; Raymo, F. M.; Stoddart, J. F.; Williams, D. J. *J. Org. Chem.* **1996**, *61*, 9591−9595. (c) Sue, C.-H.; Basu, S.; Fahrenbach, A. C.; Shveyd, A. K.; Dey, S. K.; Botros, Y. Y.; Stoddart, J. F. *Chem. Sci.* **2010**, *1*, 119−125.

(21) Förster, T.; Kasper, K. *Z. Elektrochem.* **1955**, *59*, 976−980.